AIP | Journal of Applied Physics

Relaxor ferro- and paraelectricity in anisotropically strained SrTiO3 films

R. Wördenweber, J. Schubert, T. Ehlig, and E. Hollmann

Citation: Journal of Applied Physics **113**, 164103 (2013); doi: 10.1063/1.4802676
View online: http://dx.doi.org/10.1063/1.4802676
View Table of Contents: http://scitation.aip.org/content/aip/journal/jap/113/16?ver=pdfcov
Published by the AIP Publishing

Relaxor ferro- and paraelectricity in anisotropically strained $SrTiO_3$ films

R. Wördenweber,[a] J. Schubert, T. Ehlig, and E. Hollmann
Peter Grünberg Institute (PGI) and JARA-Fundamentals of Future Information Technology, Forschungszentrum Jülich, D-52425 Jülich, Germany

(Received 4 February 2013; accepted 8 April 2013; published online 26 April 2013)

The ferroelectric properties of anisotropically strained $SrTiO_3$ films are analyzed by detailed measurements of the complex dielectric constant as function of temperature, frequency, bias voltage, and electric field direction. At low temperatures, strain induces a *relaxor-ferroelectric phase* that persists up to room temperature. The transition temperature and characteristic parameters (e.g., Curie temperature, static freezing temperature, degree of diffuseness of the phase transition, activation energy) of the relaxor phase depend strongly on the orientation of the electric field and, therefore, on the amount of structural strain in the given electric field direction. Also above the ferroelectric transition temperature, a relaxation of the permittivity is visible, i.e., the strain causes a *relaxor-paraelectric behavior*. Only at high enough temperatures, the relaxation time constant tends to zero and the "*classical" dielectric state* is obtained. Frequency and time dependent relaxation experiments demonstrate an extremely large distribution of the relaxation rates in both relaxor states (ferroelectric and paraelectric), which is indicative for the large distribution in the mobility of polar $SrTiO_3$ regions with randomly distributed directions of dipole moments in the film. The large distribution might be taken as an indication for a large distribution in size and orientation of nanosize domains in the anisotropically strained $SrTiO_3$ film. © *2013 AIP Publishing LLC*.
[http://dx.doi.org/10.1063/1.4802676]

I. INTRODUCTION

Pseudomorphous strained-layer epitaxial growth has quickly turned from a mere curiosity into a major technology for advanced semiconductor devices for solid state research. It has been demonstrated that mechanical strain can have dramatic effects on electronic and magnetic properties of thin films. Significant effects have not only been observed in semiconductor films for which the strain affects key material properties including the energy gap and effective mass—and, thus, the mobility—of the charge carriers. Prominent examples are also the strain-induced enhancement of magnetization observed in ultrathin spinel ferrite films[1,2] and the strain induced enhancement of the ferroelectricity transition temperature in perovskite ferroelectric films.[3,4]

For heteroepitaxially grown thin films, mechanical stress is naturally induced by the underlying substrate. The stress is caused by the lattice mismatch and the differences in thermal expansion coefficients between the substrate and the film. It naturally leads to strain in the layer that results in structural modifications of the film ranging from (i) the development of defects like point defects, dislocations, voids, or even cracks;[5–7] (ii) structural transitions as observed in spinel ferrites $NiFe_2O_4$ or $CoFe_2O_4$ that undergo a transition from an inverse spinel structure (without strain) to the normal spinel structure (with stain);[8] or (iii) modification of the lattice constants as observed in strained Si films and strained perovskites.[9–11] Moreover, combinations of these different structural modifications are very likely.

Most interesting and even more complex is the combination of substrate and film with different crystallographic symmetries. In this case the structural mismatch will be different in different crystallographic directions. As a result, not only the structural but also the electromechanical properties of the layer might be different in different crystallographic directions. An ideal candidate to study this effect is provided by the growth of a nominally cubic ferroelectric perovskite (e.g., $SrTiO_3$) on a non-cubic substrate. Different non-cubic substrates are suitable for heteroepitaxial growth of $SrTiO_3$ ranging from orthorhombic perovskites (e.g., $NdGaO_3$ or $DyScO_3$ (Ref. 3)) to hexagonal sapphire.[4] Since the onset of polarization in ferroelectric materials is generally accompanied by a spontaneous strain, applied stress influences the stability of the ferroelectric phases which affects the ferroelectric transition temperature as well as the dielectric and electromechanical properties.[3,4,12–22] Pure unstrained $SrTiO_3$ is a so-called incipient ferroelectric, i.e., due to quantum fluctuations of atomic positions the ferroelectric transition is suppressed down to zero-temperature. In thin films, in-plane strain can shift the ferroelectric transition temperature by up to hundreds of degrees,[3,4] in accordance with thermodynamic theory.[19,20,22] However, the existing thermodynamic predictions are based on a uniform in-plane biaxial strain state, which is reasonable for films on substrates with cubic lattice structure or films with a significant level of relaxation.

In this paper, ferroelectric properties of anisotropically strained $SrTiO_3$ on $DyScO_3$ substrates are analyzed and discussed. The dependence of the complex dielectric constant on temperature, frequency, bias voltage, and electric field direction provides detailed information about the underlying ferroelectricity and its modification due to the anisotropic strain in the $SrTiO_3$ films.

[a]Author to whom correspondence should be addressed. Electronic mail: r.woerdenweber@fz-juelich.de

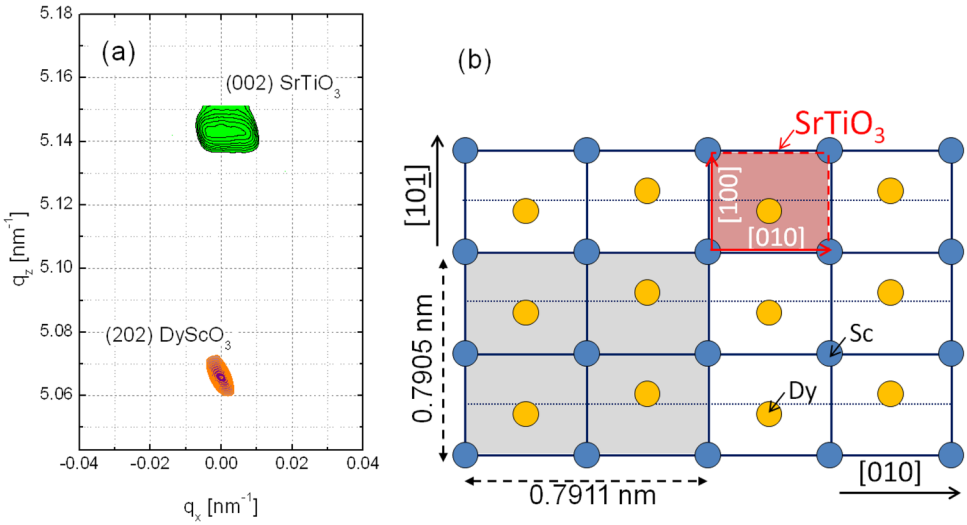

FIG. 1. (a) X-ray RSM measurement of (002) $SrTiO_3$ taking the Bragg reflection of the (202) $DyScO_3$ as a reference and (b) schematic of the in-plane rectangular surface of the (101) $DyScO_3$ including the area spanned by the $DyScO_3$ lattice vectors [010] and [10$\bar{1}$] and the orientation of the distorted unit cell of $SrTiO_3$.

II. SAMPLE PREPARATION AND EXPERIMENTAL TECHNIQUES

$SrTiO_3$ films are grown on (101)$DyScO_3$ via pulsed laser deposition using a stoichiometric $SrTiO_3$ target, a substrate heater temperature of 850 °C, O_2 process gas at a pressure of 1 Pa, a laser power of ~5 J/cm^2 at the target, and 10 Hz laser repetition rate. The resulting growth rate is ~180 nm/min. In order to avoid the formation of cracks in the $SrTiO_3$ films,[6] layer thicknesses below the critical thickness of ~120 nm are chosen.

X-ray reciprocal space mapping (RSM) is used to demonstrate the epitaxial film growth and to analyze the crystalline properties of substrate and film in detail. The $DyScO_3$ substrates have an orthorhombic $GdFeO_3$ crystal structure with space group *Pnma*. The lattice constants a = 0.5727 nm, b = 0.7911 nm, and c = 0.5449 nm (obtained from X-ray RSM) are in good agreement with literature values.[23] Slight differences in $DyScO_3$ lattice constants are generally attributed to small stoichiometry differences, as has been noted also in other $GdFeO_3$-type compounds.[24] Moreover, in case of $DyScO_3$ the optimal composition at which the compound melts congruently is slightly dysprosium poor compared to the stoichiometric Dy:Sc = 1:1 composition.[25]

The $DyScO_3$ substrate is cut along the (101) plane which results in a rectangular surface net spanned by the [10$\bar{1}$] and [010] $DyScO_3$ vectors that nearly match the cubic lattice of $SrTiO_3$ (see Fig. 1(b)). The X-ray RSM measurements reveal an epitaxial growth of $SrTiO_3$ on (101) $DyScO_3$ (Fig. 1(a)). The nominally cubic $SrTiO_3$ adapts the in-plane rectangular lattice structure of $DyScO_3$. The in-plane primitive translation vectors [100] and [010] of the $SrTiO_3$ are elongated and oriented along the [10$\bar{1}$] and [010] $DyScO_3$ directions, respectively (see Fig. 1(b)). The nominal in-plane lattice mismatch $\beta := (a_{STO,lit} - a_{DSO}/2)/a_{STO,lit}$ between film and substrate is different for the different crystalline directions (see Table I), i.e., $\beta = -1.24\%$ and -1.31% for the short ([10$\bar{1}$] $DyScO_3$) and the long ([010] $DyScO_3$) axes, respectively (a refers to the lattice parameter of the given compound denoted by the subscripts $_{DSO}$ or $_{STO}$ and the subscript $_{lit}$ denotes the literature values of the unstrained oxide). Due to the lattice mismatch, the resulting strain $\eta := (a_{STO} - a_{STO,lit})/a_{STO,lit}$ of the $SrTiO_3$ is expected to depend on the crystalline direction. Experimentally (via RSM) determined values for η are given in Table I. As a consequence of Poisson's ratio, the positive (tensile) strain of the in-plane directions (0.95% for [100] $SrTiO_3$ and 1.03% for [010] $SrTiO_3$) results in a negative (compressive) strain of the out-of-plane direction (-0.39% for [001] $SrTiO_3$).

In order to investigate the in-plane dielectric properties of the $SrTiO_3$ films, planar capacitors in the form of interdigitated electrodes (IDE) are employed. The IDEs are obtained via lift-off lithography technique and deposition of a 50 nm thick Nb/Au layer via sputter technology. The thin (5 nm) Nb layer provides a perfect adhesion of the electrodes on the $SrTiO_3$ layer. Typical Nb/Au electrodes are shown in Fig. 2. In order to obtain a reliable and large signal, a relatively large gap size $s = 5\ \mu$m is chosen that is compensated by large length $d = 700\ \mu$m of the individual IDE's fingers and a large number of fingers resulting in an effective length of the capacitor of

TABLE I. Lattice parameter, mismatch, and strain of a 105 nm thick $SrTiO_3$ film epitaxially grown on a (101)$DyScO_3$ substrate. The nominal lattice mismatch β and the strain η of the $SrTiO_3$ film are calculated using experimental data (X-ray RSM) and a literature value of $a_{STO} = 0.39042$ nm for the unstrained cubic $SrTiO_3$ lattice.

	Direction		Lattice parameter (nm)			
	$DyScO_3$	$SrTiO_3$	$DyScO_3$	$SrTiO_3$	Lattice mismatch, β (%)	Strain, η (%)
In-plane	[10$\bar{1}$]	[100]	0.7905	0.39411	−1.24	0.95
	[010]	[010]	0.7911	0.39444	−1.31	1.03
Out-off plane		[001]		0.38889		−0.39

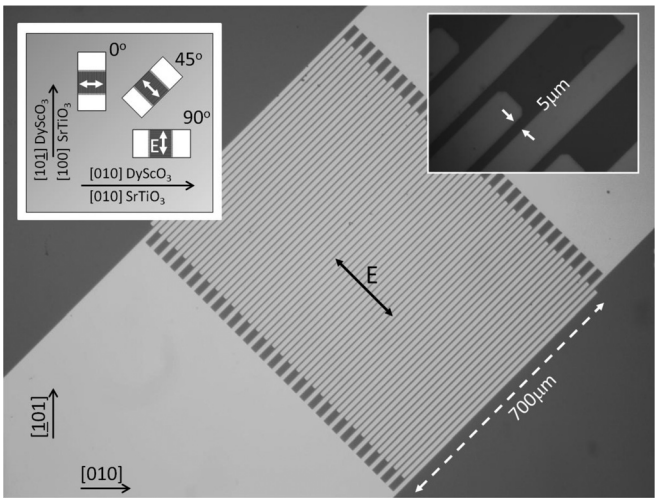

FIG. 2. Images (main figure and right inset) of the interdigitated electrode structure for the 45° oriented IDE. The left inset shows the different orientations of the three IDEs on a $SrTiO_3$ film on (101) $DyScO_3$. Additionally, the direction of the electric field E and the crystallographic orientation of the $SrTiO_3$ and $DyScO_3$ are given.

44.1 mm (see Fig. 2). In order to suppress stray fields, the gap is strongly extended at the end of each finger (see inset of Fig. 2). This guarantees that the electric field E is oriented perpendicular to the direction of the fingers.

Three identical IDE structures with different orientations 0°, 45°, and 90° of the electric field E with respect to the [010] axis (long axis) of the $DyScO_3$ substrate are patterned on each sample. Thus, the electronic properties of the $SrTiO_3$ layer can be probed at various angles in the plane of the film, i.e., for E//[010]$DyScO_3$ (0°), E//[10$\bar{1}$]$DyScO_3$ (90°), and E//[$\bar{1}$11]$DyScO_3$ (45°), respectively (Fig. 2).

The dielectric properties are analyzed as function of temperature (20 K to 320 K), frequency (20 Hz to 2 MHz), and dc-bias voltage (−40 V to 40 V) using a high precision capacitance meter (HP4278A, 1 kHz/1 MHz) and a LCR meter (ST2826A, 20 Hz–2 MHz). The in-plane real part of the dielectric constant ε' of the $SrTiO_3$ films is calculated using a *partial capacitance model*.[26–28] The model is based on conformal mapping and allows to evaluate the capacitive contribution of all components (especially substrate and ferroelectric film) of planar structures. The model strictly valid for our geometry is the model of Gevorgian *et al.*[27] However, due to the geometrical design of the IDE and the large permittivity of the $SrTiO_3$ films in comparison to that of the substrate, all three models yield nearly identical results. The dielectric loss tangent tan $\delta = \varepsilon'/\varepsilon''$ of the $SrTiO_3$ layer is obtained via correction of the total loss tangent using an identical reference sample without $SrTiO_3$ layer.

III. EXPERIMENTAL RESULTS

The dielectric properties are determined for the different in-plane directions using the IDEs with different orientations. The data are analyzed according to the planar capacitance model using a reference measurement on identical IDE structures on a (101) $DyScO_3$ substrate without $SrTiO_3$ film. Fig. 1 shows the resulting in-plane dielectric constant ε' and loss tangent tan δ of a 105 nm thick $SrTiO_3$ film as function of temperature for the different orientations measured at 1 MHz for zero dc-bias $V_{dc} = 0$ V and, for comparison, a dc-bias of $V_{dc} = 40$ V.

The most striking features of this figure are as follows:

- Without dc-bias the dielectric properties (permittivity and loss tangent) strongly depend on the orientation of the electric field. For instance, a distinct peak in the permittivity and loss tangent is visible with a maximum at a temperature that is (a) close to room temperature and (b) depends on the orientation of the applied electric field.
- With dc-bias the dielectric properties are nearly identical for all orientations of the electric field.
- Moreover, already a relatively small dc-bias (40 V over a gap of 5 μm, i.e., 8 V/μm) leads to extremely large reduction of the permittivity (i.e., extremely large tunability) and losses, and a complete extinction of the peaks in the temperature dependence of ε' and tan δ (see Fig. 3).

These different features, including a detailed analysis of the frequency and dc-bias dependence of the dielectric properties of the different IDE orientations, will be discussed in detail in the following sections.

A. Strain induced phase transition

Pure unstrained $SrTiO_3$ is a quantum paraelectric material. Quantum fluctuations of atomic positions suppress the

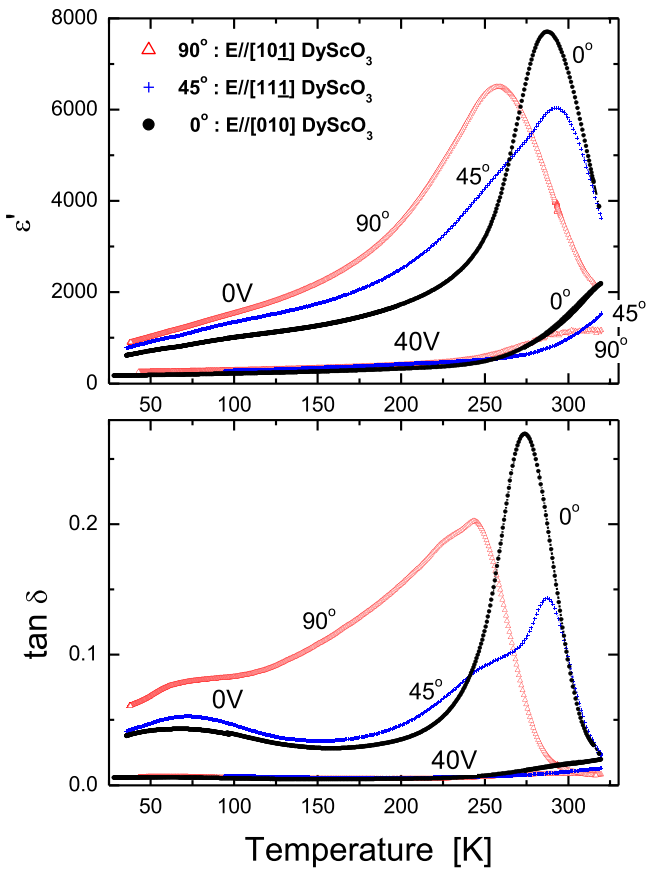

FIG. 3. Temperature dependence of the in-plane dielectric constant (a) and loss tangent (b) of a 105 nm thick $SrTiO_3$ film measured at 1 MHz for different orientations of the electric field E, zero-dc-bias (upper curves) and a dc-bias of $V_{dc} = 40$ V (lower curves), respectively.

TABLE II. Angular dependence of characteristic parameters of a strained $SrTiO_3$ film on $DyScO_3$. The different characteristic temperatures are the temperature T_{max} of maximum permittivity ε_{max}, the Curie temperature T_c obtained from the Curie-Weiss fit for $T > T_{max}$, the Burns temperature T_B at which the permittivity deviates from the Curie-Weiss behavior, and the static freezing temperature T_{VF} obtained from the Vogel-Fulcher equation fit (Eq. (2)), respectively. Furthermore, σ, γ, and E_a represent the degree of diffuseness of the phase transition, the degree of dielectric relaxation, and the activation energy obtained from the relaxation equation (Eq. (1)) and the Vogel-Fulcher equation fit (Eq. (2)), respectively. It should be noted that due to experimental accuracy all values for degree of dielectric relaxation should be considered to be $\gamma \approx 2$.

	Orientation	T_{max} (K)	T_c (K)	T_B (K)	T_{VF} (K)	ε_{max}	γ	σ [K]	E_a [meV]
90°	E//[10$\underline{1}$] $DyScO_3$	258	266 ± 2	292	230.2	6504	2.07	35.0	32
45°	E//[11$\underline{1}$] $DyScO_3$	292.5	290 ± 2	308	273.7	6032	2.18	32.1	16
0°	E//[010] $DyScO_3$	288	294.7 ± 3	315	276.5	7705	2.01	23.3	12

ferroelectric transition down to zero-temperature leading to so-called incipient ferroelectricity.[29–31] The permittivity of unstrained $SrTiO_3$ increases from $\varepsilon' \approx 300$ at room temperature to $\varepsilon' \approx 25\,000$ at 4 K; however, polarization-electric-field hysteresis—a signature of ferroelectricity—does not develop even at lowest temperatures. In the dielectric regime, the temperature-dependence of the permittivity is described by the Curie-Weiss law, $\varepsilon'(T) \propto (T-T_c)^{-1}$ with a Curie temperature for unstrained pure $SrTiO_3$ of $T_c \approx 49$ K.[32] However, the quantum paraelectric state is very sensitive to small perturbations. Ferroelectricity can be induced among others by mechanical stress.[16] The ability to tailor the strain in epitaxially grown $SrTiO_3$ films offers a tool to induce ferroelectricity up to high temperatures. This has been predicted[19,20] and experimentally demonstrated.[3,4]

First indication for a phase transition from a dielectric (or paraelectric) to a ferroelectric (or relaxor-ferroelectric) state is given by the pronounced peak in the temperature dependence of the dielectric constant that suggests a shift of the Curie temperature to higher temperatures. An unambiguous proof would be provided by the hysteretic behavior of the electric field dependence of the permittivity.

For our sample, both characteristic temperatures, the temperature T_{max} (maximum in the ε'-versus-T plot) and the Curie temperature T_c (obtained from a Curie-Weiss fit of the permittivity for $T > T_{max}$), are close to room temperature (see Table II). The exact values for T_{max} and T_c strongly depend on the orientation of the IDE, i.e., on the electric field orientation. Comparing the two principal $SrTiO_3$ in-plane lattice directions, T_{max} and T_c are higher for the electric field oriented along the longer crystalline axis (0° IDE: $T_{max} = 288$ K and $T_c \approx 295$ K) than for the field direction along the shorter axis (90° IDE: $T_{max} = 258$ K and $T_c \approx 266$ K). This agrees with the theoretical prediction[20] that the transition temperature increases with increasing strain. Already the small difference in strain ($\Delta\eta \approx 0.08\%$) leads to a shift of T_{max} and T_c of about 30 K.

The 45° oriented IDE shows a peak position and Curie temperature close to that of the 0° IDE (with the higher T_{max} and T_c values). However, a closer look on the data reveals, that in this case the temperature dependence has to be fitted with two peaks at peak positions identical to that of the 0° and 90° IDEs. This can nicely be seen in Fig. 4 which shows the temperature dependence of tan δ for different bias voltages for the 45° IDE. The two peak positions for the 0° and 90° IDEs are indicated in the figure. The dielectric properties (ε' and tan δ) of IDE 45° sample both peaks.

A direct test of the transition to the ferroelectric phase is provided by permittivity-versus-bias characteristics. Fig. 5(a) shows a set of ε'-vs-V_{dc} characteristics for one of the IDEs (similar sets of characteristics are recorded for all IDEs). All characteristics are hysteretic. However, at low temperatures butterfly-shaped hysteretic curves are obtained with maxima at non-zero bias, whereas at high temperatures the curves become dome-shaped with a maximum at zero bias for increasing and decreasing bias voltage. The low-temperature behavior is characteristic for a ferroelectric state or relaxor ferroelectric state. With increasing temperature, the peak position of the ε'-vs-V_{dc} characteristic shifts towards zero-voltage (see Fig. 5(b)). Finally, at high enough temperature the maxima in ε'-vs-V_{dc} (for increasing and decreasing bias) are obtained at zero-bias, i.e., the sample becomes paraelectric. The temperature of the transition ranges between 260 K and 310 K (see Fig. 5(b)), which coincides with the prediction of the transition temperature obtained from the Curie temperature T_c and T_{max}. However, even in the paraelectric state a relaxation of the permittivity (and loss angle) is observed. This is demonstrated among others by the hysteretic type of the ε'-vs-V_{dc} characteristics recorded even at the highest temperatures (e.g., data for 300 K in Fig. 5(a)). In analogy to the *relaxor-ferroelectric phase*, this phase could be called a *relaxor-paraelectric phase*. We will later show that in our samples relaxation of the permittivity persists up to temperatures of approximately 330 K.

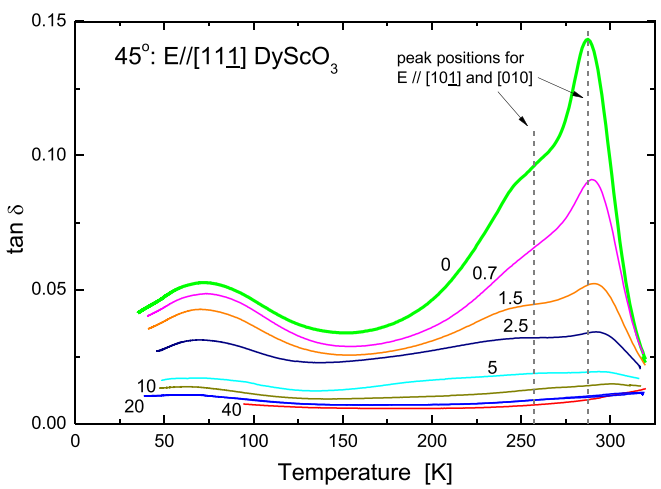

FIG. 4. Temperature dependence of the loss tangent for the 45° oriented IDE for different dc-bias voltage. The numbers represent the bias voltage, the dashed lines mark the peak positions for the 0° and 90° IDEs.

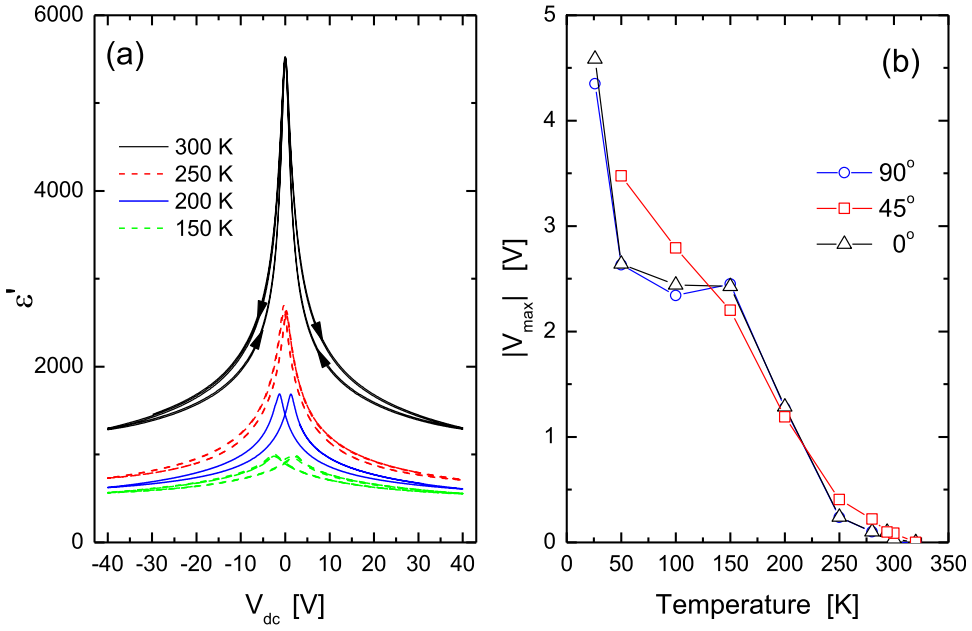

FIG. 5. (a) Permittivity as function of dc-bias for the 0° IDE (E//[10$\bar{1}$] $DyScO_3$) and (b) temperature dependence of the maximum bias voltage V_{max} which denotes the position of the maxima in the permittivity-versus-bias characteristic.

In conclusion of this section, we can state that there is strong evidence for a strain-induced phase transition from a paraelectric-type phase to a ferroelectric-type phase at temperatures close to room temperature in our epitaxial $SrTiO_3$ films on (101)$DyScO_3$ substrates. The exact transition temperature depends on the orientation of the applied electric field and can be correlated with the strain of the $SrTiO_3$ lattice in the direction of the electric field. Moreover, there is strong evidence that both phases (paraelectric and ferroelectric) are relaxor-type phases. Relaxor ferroelectric behavior has been reported for similar systems.[9,33] It is examined for our samples in more detail in Sec. III B.

B. Relaxor and frequency dependent experiments

Relaxor ferroelectrics or relaxors represent a class of disordered ferroelectric crystals with particular structure and properties. At high temperature, they exist in a non-polar paraelectric phase that is similar in many respects to the paraelectric phase of classical ferroelectrics. Upon cooling, they transform into the ergodic relaxor state which is caused by polar nanoregions with randomly distributed directions of dipole moments. This transformation occurs at the so-called Burns temperature T_B which is defined by the temperature at which the permittivity deviates from the Curie-Weiss behavior (values for T_B are given in Table II). In principle, this transition is not considered to be a structural phase transition since it is not accompanied by any change of crystal structure on macroscopic or mesoscopic scale. Nevertheless, the polar nanoregions strongly affect the ferroelectric properties of the crystalline material. For this reason, the state of the crystalline material at $T < T_B$ is often considered to be a new phase, the *relaxor ferroelectric phase*.

At temperatures close to the Burns temperature, the polar nanoregions are mobile and their behavior is ergodic. On cooling, their dynamics slows down enormously and at a low enough temperature (typically hundreds degrees below T_B), they become frozen into a nonergodic state. The phase transition at T_B represents a diffuse phase transition that can be scaled according to the empirical Lorentz-type relation,[34]

$$\frac{\varepsilon'_{\max}}{\varepsilon'} - 1 = \frac{(T - T_{\max})^{\gamma}}{2\sigma}, \tag{1}$$

for $T > T_{max}$, $\varepsilon'_{max} = \varepsilon'(T_{max})$, and σ and γ representing the degree of diffuseness of the phase transition and the degree of dielectric relaxation, respectively. For a classical ferroelectric, a sharp phase transition with $\gamma = 1$ is expected. Diffusing of the phase transition leads to an increase of γ up to 2. Larger values of γ express "more relaxor-type behavior" of the ferroelectric and values of $\gamma = 2$ are considered to be characteristic for relaxor ferroelectrics[34,35] The Lorentz-type scaling of the transition is demonstrated for our $SrTiO_3$ film in a double logarithmic plot of the normalized permittivity $(\varepsilon'_{max} - \varepsilon')/\varepsilon'$ versus $(T - T_{max})$ in Fig. 6. The slope of the linear dependence yields values of $\gamma \approx 2$ (Table II) and thus strongly supports the assumption of a relaxor-type transition at T_B for our samples.

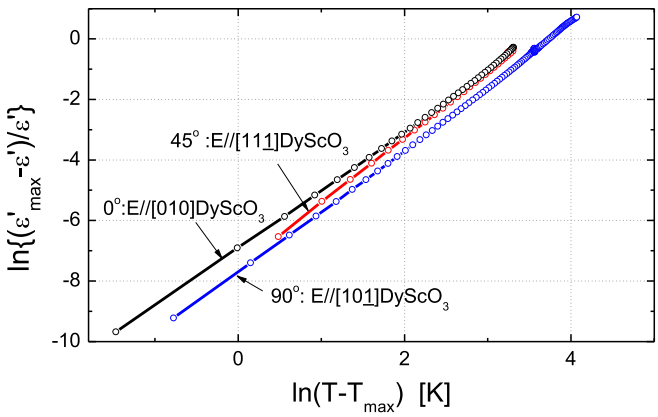

FIG. 6. Double logarithmic plot of the reduced and normalized permittivity versus reduced temperature at the phase transition ($T > T_{max}$) for the IDEs with different orientations of the electric field. The fits according to Eq. (1) reveal values of $\gamma \approx 2$ and $\sigma \approx 23$–35 K (exact values are given in Table II).

Another characteristic feature of relaxor ferroelectrics is provided by a characteristic frequency dependence of the dielectric properties which is most prominent at the transition to the relaxor ferroelectric state. Fig. 7(a) shows the temperature dependence of the permittivity for different frequencies (20 Hz to 2 MHz) for the three different orientations of the IDE. Especially at the peak in ε'—i.e., close to the transition—large differences in the permittivity are recorded for different frequencies. With decreasing frequency the permittivity increases. The frequency dispersion in the dielectric constant clearly indicates relaxor behavior. The convergence of the permittivity data above T_{max} demonstrates that the dispersion is not an artifact of the experiments, e.g., caused by space charge polarizability. The frequency dependence of the maximum is characteristic of many relaxor ferroelectrics[36,37] and is described by the Vogel-Fulcher equation,[38]

$$f = (2\pi\tau_o)^{-1}\exp\left[-\frac{E_a}{k_B(T_{\max} - T_{VF})}\right], \qquad (2)$$

with the attempt frequency $f_o = (2\pi\tau_o)^{-1}$, the activation energy E_a, Boltzmann constant k_B, and the static freezing temperature T_{VF}.

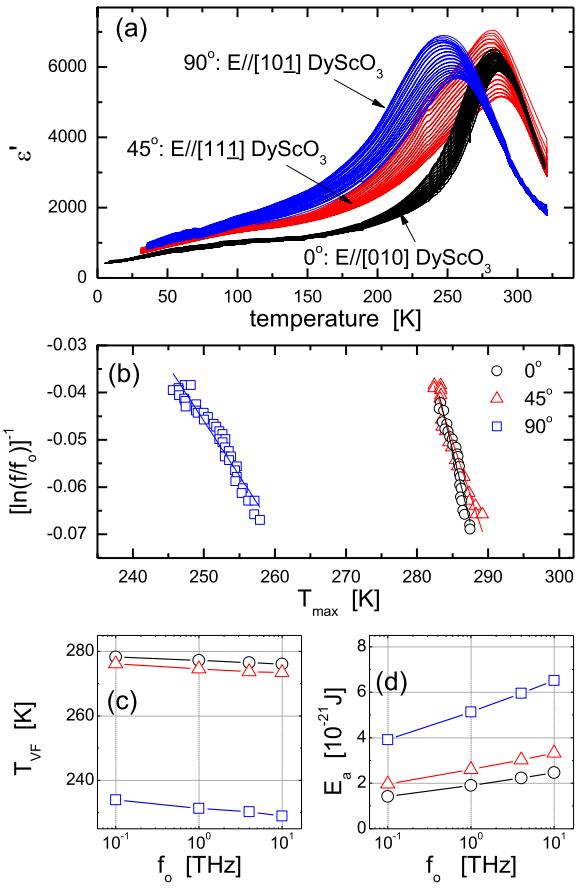

FIG. 7. *Vogel-Fulcher equation fits of T_{max} and E_a* (Eq. (2)): (a) Permittivity as function of temperature for the different orientations and frequencies ranging from 20 Hz (largest permittivity) to 2 MHz (smallest permittivity), (b) plot of the reduced frequency $[(f/f_o)]^{-1}$ as function of the temperature T_{max} according to the Vogel-Fulcher equation (Eq. (2)) using an attempt frequency of $f_o = 4$ GHz, (c) the resulting static freezing temperature T_{VF}, and (d) activation energy E_a for different choices of attempt frequencies $f_o = (2\pi\tau_o)^{-1}$. The lines in (b) indicate the linear fit of the data for an attempt frequency of $f_o = 4$ GHz. The symbols in (b)–(d) represent 0° IDE (circles), 45° IDE (triangles), and 90° (squares), respectively.

Vogel-Fulcher equation fits of our permittivity data measured for frequencies ranging between 20 Hz and 2 MHz are given in Fig. 7(b). They show the predicted linear relation between the reduced frequency $[\ln(f/f_o)]^{-1}$ and T_{max}. Inserting a reasonable value for the attempt frequency f_o (typical value: 1–10 GHz) yields values for the static freezing temperature T_{VF} and activation energy E_a. Figs. 7(c) and 7(d) demonstrate that freezing temperature and activation energy do not depend strongly on the choice of the attempt frequency, but they depend strongly on the orientation of the electric field with respect to the strain. For instance, for $f_o = 4$ GHz (see also Table II), we obtain values of $T_{VF} \approx 230$ K and $E_a \approx 32$ meV for the 90° IDE and $T_{VF} \approx 276.5$ K and $E_a \approx 12$ meV for the 0° IDE. The evaluated E_a values represent typical values for the activation energy of relaxor ferroelectrics.[9,36] Also, the reduction of the activation energy for the 0° IDE (direction of the electric field parallel to the longer crystalline axis) agrees with the theoretical expectation.

At this point, we can state that all experimental results support the assumption that the strained $SrTiO_3$ films on (101) $DyScO_3$ represents a relaxor ferroelectric. Therefore, we will finally focus our attention on the tunability of the $SrTiO_3$ films and especially the relaxation effects that are visible in dc bias dependent measurements of the permittivity relaxation of the $SrTiO_3$ films.

C. Relaxation of the tunability

Figs. 8 and 9 present a more detailed analysis of the dc-bias dependence of the permittivity. Measurements at constant dc-bias voltage V_{dc} demonstrate the large tunability of our strained $SrTiO_3$ films (Fig. 8). Already a small voltage of $V_{dc} = 0.4$ V ($E_{dc} = 80$ mV/μm) yields a considerable reduction of ε', a bias of $V_{dc} = 40$ V ($E_{dc} = 8$ V/μm) reduces the permittivity by up to a factor of 10 (tunability $n = \varepsilon(0)/\varepsilon(V_{dc})$ up to 10). However, only at high temperatures ($T > 300$ K) the tuning of the $SrTiO_3$ film via dc-bias is reversible, i.e., the zero-bias permittivity is retained after removal of the dc voltage. At lower temperatures (typically 230 K–280 K), the permittivity relaxes slowly but does not reach the zero-field permittivity. At even lower temperatures ($T < 200$ K), the permittivity immediately relaxes to a value clearly below zero-field permittivity after removal of the bias voltage, i.e., a state different to the zero-bias state seems to be frozen in. The different temperature regimes are clearly visible in Fig. 8.

Fig. 9 shows the relaxation behavior of the permittivity for one of the orientation (90° IDE) in more detail. The relaxation of ε' after removal of a bias voltage (40 V is applied for 10 min) is recorded for 20 min. At the lowest temperatures (for this orientation $T < 200$ K), the removal of the dc bias causes an immediate jump to a fixed permittivity value clearly smaller than the value obtained for the zero-bias measurements (see also Fig. 8). However, no further relaxation is visible in Fig. 9 for these temperatures (it should be noted that first reliable data are collected 2 s after removal of the bias voltage). For higher temperatures, a relaxation is visible for the whole period of the recording (20 min). For the highest temperatures, the permittivity seems to asymptotically approach the final value, i.e., the

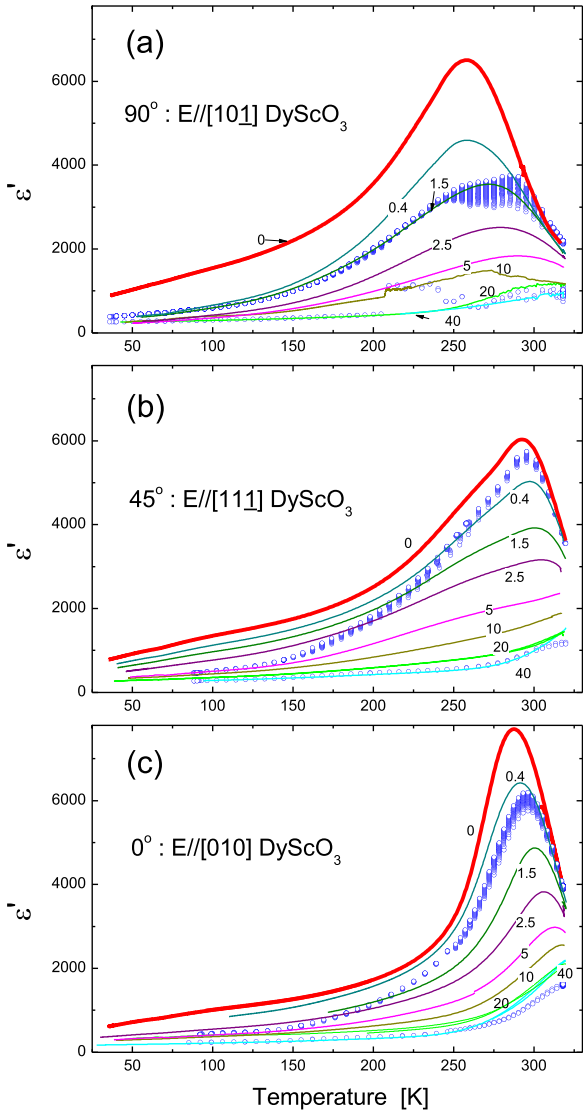

FIG. 8. Temperature dependence of the permittivity $\varepsilon'(V_{dc})$ for the different orientations of the electric field: (a) 90° IDE, (b) 45° IDE, and (c) 0° IDE. The solid lines represent measurements at constant dc bias, the bias voltage V_{dc} is given by the numbers in the figure (gap size is 5 μm). The symbols (open circles) represent relaxation measurements for which at each temperature first a bias voltage of 40 V was applied for 10 min (lower ε' values) which was then removed and the relaxation of the permittivity was recorded every 12 s for 20 min (upper set of ε' values). Different temperature regimes are visible: At low temperatures, the permittivity relaxes to a fixed value clearly below the "virgin" $\varepsilon'(0\,\text{V})$ curve, at intermediate temperature the permittivity relaxes slowly but does not reach the zero-field permittivity, only at the highest temperatures ε' relaxes immediately to the virgin zero-bias permittivity.

zero-bias permittivity. Generally, relaxation processes can be described by an exponential function that for the relaxation of the permittivity is given by

$$\varepsilon'(t) = \varepsilon'(t=\infty) + a \cdot \exp\left(-\frac{t}{\tau}\right), \tag{3}$$

with a relaxation time constant $\tau = 1/R$ that characterizes the relaxation rate R. For more complex systems, distributions of relaxation rates or stretched exponential functions[39] are necessary to describe the relaxation process. In our case, the relaxation is reasonably well described by two relaxation

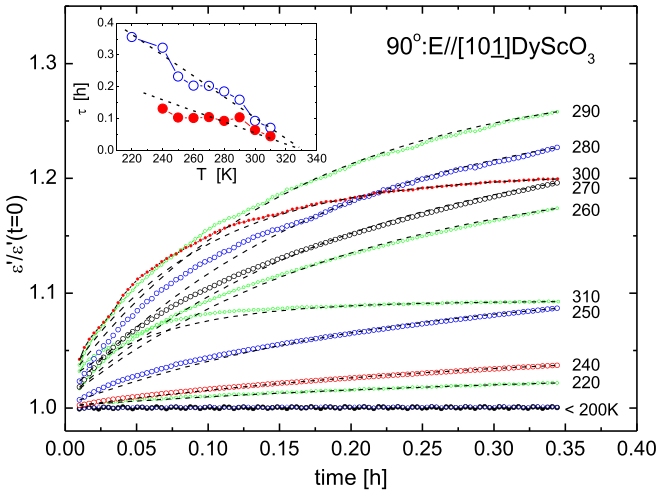

FIG. 9. Relaxation of the normalized permittivity at zero-dc-bias after applying a dc-bias of $V_{dc} = 40$ V for 10 min for the 90° IDE (bias field along the short $SrTiO_3$ axis). The symbols show the experimental data, the dashed lines represent exponential fits of the long-term relaxation according to Eq. (3), the temperatures for each measurement are given in the figure. The inset shows the relaxation time τ_1 and τ_2 obtained from the exponential fit for the short-term relaxation t < 0.15 h (solid symbols) and the long-term relaxation t > 0.15 h (open symbols), respectively.

constants τ_1 and τ_2 that characterize the short-term relaxation (t < 0.15 h) and the long-term relaxation (t > 0.15 h), respectively (see inset of Fig. 9). The relaxation time constants are very large at low temperature and tend towards zero above room temperature (approximately at 330 K) where instantaneous relaxation is expected (i.e., $R \rightarrow \infty$).

In general, relaxation times of the order of hour(s) (i.e., relaxation rates below 1 mHz) are not unusual for relaxor ferroelectrics.[40] Furthermore, large distributions of relaxation times are known, they are indicative for the large distribution in the mobility of polar $SrTiO_3$ regions with randomly distributed directions of dipole moments.[37,41] The large distribution might be taken as an indication for the large distribution in size and orientation of the micro- or even nanosize domains in the anisotropically strained $SrTiO_3$ film. Finally, even in the paraelectric state the relaxation persists. For instance, for the 90° IDE, significant relaxation with relaxation rates of $R_1 = 1/\tau_1 \approx 5$ mHz and $R_2 = 1/\tau_2 \approx 2.7$ mHz are obtained at room temperature (Fig. 9). Thus, the relaxor behavior is not restricted to the ferroelectric phase, it persists in the paraelectric regime.

IV. CONCLUSIONS

The ferroelectric properties of anisotropically strained $SrTiO_3$ films on $DyScO_3$ substrates are analyzed by detailed measurements of the complex dielectric constant as function of temperature, frequency, bias voltage, and electric field direction. It is demonstrated that at low temperatures, strain induces a *relaxor-ferroelectric phase* that persists up to temperatures around room temperature. However, also above the ferroelectric transition temperature a relaxation of the permittivity is visible, i.e., the strain causes a *relaxor-paraelectric behavior* (see Fig. 10). Only at high enough temperatures, the relaxation time constant tends to zero and the "*classical*" *dielectric state* is obtained.

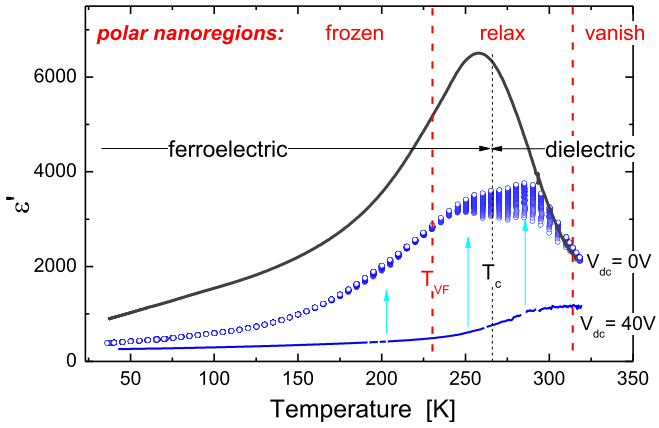

FIG. 10. The comparison of the temperature dependence of the "virgin" (i.e., initial zero-bias) permittivity (black line) and the relaxation of the permittivity after applying a dc bias demonstrates the complex behavior of the anisotropically strained $SrTiO_3$ film illustrated by the data of the 90° IDE. Only in a small temperature regime (starting at the freezing temperature T_{VF}), relaxation of the polar nanoregions is observed. At low temperature, the polar nanoregions are frozen, at high temperature the impact of the polar nanoregions vanishes. The temperature regimes of these different characteristic behaviors of the polar nanoregions do not coincide with the transition to relaxor ferroelectricity at T_c as indicated in the figure.

The characteristic parameters (e.g., Curie temperature T_c, static freezing temperature T_{VF}, degree of diffuseness of the phase transition σ, or activation energy E_a) of the relaxor phase and the phase transition depend strongly on the orientation of the electric field and, therefore, on the amount of structural strain in the given electric field direction. Already, relatively small dc bias fields lead to a complete suppression of the ferroelectric transition and a strong reduction of the anisotropy in the dielectric properties. Frequency and time dependent relaxation experiments demonstrate an extremely large distribution of the relaxation rates in the relaxor states (ferroelectric and paraelectric), which range from below 1 mHz to above 1 MHz. This is indicative for the large distribution in the mobility of polar $SrTiO_3$ regions with randomly distributed directions of dipole moments. The large distribution might be taken as an indication for the large distribution in size and orientation of the micro- or even nanosize domains in the anisotropically strained $SrTiO_3$ film.

On the one hand, the anisotropically strained $SrTiO_3$ films represent a very interesting system for analyzing and understanding of the effect of strain on structural and electromechanical properties in heteroepitaxial films in general. On the other hand, a number of structural and electronic properties might be is of interest for practical applications. These are, for instance, the large permittivity at room temperature (up to $\varepsilon' \sim 7000$ compared to $\varepsilon' \sim 300$ of unstrained $SrTiO_3$) and the large tunability at room temperature (e.g., $n(8\ V/\mu m) = \varepsilon(0)/\varepsilon(8\ V/\mu m) = 5.6$ for the 45° IDE).

ACKNOWLEDGMENTS

The authors would like to thank R. Kutzner, T. Grellmann, K. Greben, H. P. Bochem, M. Nonn, J. Schwarzkopf, and A. Offenhäusser for their valuable support.

[1]U. Lüders, M. Bibes, J.-F. Bobo, M. Cantoni, R. Bertacco, and J. Fontcuberta, Phys. Rev. B **71**, 134419 (2005).
[2]F. Rigato, S. Estradé, J. Arbiol, F. Peiró, U. Lüders, X. Martí, F. Sánchez, and J. Fontcuberta, Mater. Sci. Eng., B **144**, 43 (2007).
[3]J. H. Haeni, P. Irvin, W. Chang, R. Uecker, P. Reiche, Y. L. Li, S. Choudhury, W. Tian, M. E. Hawley, B. Craigo, A. K. Tagantsev, X. Q. Pan, S. K. Streiffer, L. Q. Chen, S. W. Kirchoefer, J. Levy, and D. G. Schlom, Nature **430**, 758 (2004).
[4]R. Wördenweber, E. Hollmann, R. Kutzner, and J. Schubert, J. Appl. Phys. **102**, 044119 (2007).
[5]A. G. Zaitsev, G. Ockenfuß, and R. Wördenweber, Inst. Phys. Conf. Ser. **158**, 25 (1997).
[6]E. Hollmann, J. Schubert, R. Kutzner, and R. Wördenweber, J. Appl. Phys. **105**, 114104 (2009).
[7]M. D. Biegalski, D. D. Fong, J. A. Eastman, P. H. Fuoss, S. K. Streiffer, T. Heeg, J. Schubert, W. Tian, C. T. Nelson, X. Q. Pan, M. E. Hawley, M. Bernhagen, P. Reiche, R. Uecker, S. Trolier-McKinstry, and D. G. Schlom, J. Appl. Phys. **104**, 114109 (2008).
[8]D. Fritsch and C. Ederer, Appl. Phys. Lett. **99**, 081916 (2011).
[9]H. W. Jang, A. Kumar, S. Denev, M. D. Biegalski, P. Maksymovych, C. W. Bark, C. T. Nelson, C. M. Folkman, S. H. Baek, N. Balke, C. M. Brooks, D. A. Tenne, D. G. Schlom, L. Q. Chen, X. Q. Pan, S. V. Kalinin, V. Gopalan, and C. B. Eom, Phys. Rev. Lett. **104**, 197601 (2010).
[10]R. Wördenweber, T. Grellmann, K. Greben, J. Schubert, R. Kutzner, and E. Hollmann, Ferroelectrics **430**, 57–64 (2012).
[11]J. Schwarzkopf, M. Schmidbauer, A. Duk, A. Kwasniewski, S. B. Anooz, A. Devi, and R. Fornari, "Strain induced phase transitions in NaNbO3 epitaxial thin films grown by MOCVD," J. Appl. Crystallogr. **45**, 1015 (2012).
[12]D. Bancroft, Phys. Rev. **53**, 587 (1938).
[13]A. F. Devonshire, Adv. Phys. **3**, 85 (1954).
[14]P. W. Forsbergh, Jr., Phys. Rev. **93**, 686 (1954).
[15]G. A. Samara, Ferroelectrics **2**, 277 (1971).
[16]H. Uwe and T. Sakudo, Phys. Rev. B **13**, 271 (1976).
[17]G. A. Rossetti, K. Kushida, and L. E. Cross, Appl. Phys. Lett. **59**, 2524 (1991).
[18]K. Abe, N. Yanase, K. Sano, M. Izuha, N. Fukushima, and T. Kawakubo, Integr. Ferroelectr. **21**, 197 (1998).
[19]N. A. Pertsev, A. G. Zembilgotov, and A. K. Tagantsev, Phys. Rev. Lett. **80**, 1988 (1998).
[20]N. A. Pertsev, A. K. Tagantsev, and N. Setter, Phys. Rev. B **61**, R825 (2000); **65**, 219901(E) (2002).
[21]K. J. Choi, M. D. Biegalski, Y. L. Li, A. Sharan, J. Schubert, R. Uecker, P. Reiche, Y. B. Chen, X. Q. Pan, V. Gopalan, L.-Q. Chen, D. G. Schlom, and C. B. Eom, Science **306**, 1005 (2004).
[22]D. G. Schlom, L.-Q. Chen, C.-B. Eom, K. M. Rabe, S. K. Streiffer, and J.-M. Triscone, Annu. Rev. Mater. Res. **37**, 589–626 (2007).
[23]M. Schmidbauer, A. Kwasniewski, and J. Schwarzkopf, Acta Crystallogr. **68**, 8–14 (2012).
[24]R. J. Hill and I. Jackson, Phys. Chem. Miner. **17**, 89 (1990).
[25]R. Uecker, M. Albrecht, B. Velickov, M. Bernhagen, and D. G. Schlom, J. Cryst. Growth **295**, 84 (2006).
[26]O. G. Vendik, S. P. Zubko, and M. A. Nikol'skii, Tech. Phys. **44**, 349–355 (1999); O. G. Vendik and M. A. Nikol'skii, Tech. Phys. **46**, 112–116 (2001).
[27]S. S. Gevorgian, T. Martinsson, P. L. Linner, and E. L. Kollberg, IEEE Trans. Microwave Theory Tech. **44**, 896 (1996).
[28]E. Chen and S. Y. Chou, IEEE Trans. Microwave Theory Tech. **45**, 939 (1997).
[29]K. A. Müller and H. Burkard, Phys. Rev. B **19**, 3593 (1979).
[30]W. Zhong and D. Vanderbilt, Phys. Rev. B **53**, 5047 (1996).
[31]J. Hemberger, P. Lunkenheimer, R. Viana, R. Böhmer, and A. Loidl, Phys. Rev. B **52**, 13159 (1995).
[32]M. Trainer, Eur. J. Phys. **21**, 459–464 (2000).
[33]M. Tyunina and J. Levoska, Phys. Rev. B **70**, 132105 (2004).
[34]A. A. Bokov and Z.-G. Ye, Solid State Commun. **116**, 105 (2000).
[35]A. A. Bokov, Y. H. Bing, W. Chen, Z. G. Ye, S. A. Bogatina, I. P. Raevski, S. I. Raevskaya, and E. V. Sahkar, Phys. Rev. B **68**, 052102 (2003).
[36]D. Viehland, S. J. Jang, L. E. Cross, and M. Wuttig, J. Appl. Phys. **68**, 2916 (1990).
[37]A. A. Bokov and Z.-G. Ye, J. Mater. Sci. **41**, 31–52 (2006).
[38]H. Vogel, Phys. Z. **22**, 645 (1921); G. S. Fulcher, J. Am. Ceram. Soc. **8**, 339 (1925).
[39]R. Kohlrausch, Ann. Phys. Chem. **91**, 56–82, 179–213 (1854).
[40]V. V. Gladkiĭ, V. A. Kirkov, E. S. Ivanova, and T. R. Volk, Phys. Solid State **48**, 1106 (2006).
[41]L. E. Cross, Ferroelectrics **76**, 241–267 (1987).